Journal of *Marine Science and Engineering*

MDPI

Article

Robust Positioning Estimation for Underwater Acoustics Targets with Use of Multi-Particle Swarm Optimization

Xiyun Ge [1,2,*], Hongkun Zhou [1,2], Junbo Zhao [1,2], Xiaowei Li [1,2], Xinyu Liu [1,2], Jin Li [1,2] and Chengming Luo [3]

[1] China Ship Scientific Research Center, Wuxi 214081, China; zhouhk@126.com (H.Z.); lixiaoweihu@163.com (X.L.); 1903635173@hrbeu.edu.cn (X.L.); 15261583966@163.com (J.L.)
[2] Taihu Laboratory of Deepsea Technological Science, Wuxi 214081, China
[3] Ocean College, Jiangsu University of Science and Technology, Zhenjiang 212100, China; chengmingluo@126.com
* Correspondence: gexiyuncssrc@126.com

Abstract: With the extensive application of sensor technology in scientific ocean research, ocean resource exploration, underwater engineering construction, and other fields, underwater target positioning technology has become an important support for the ocean field. This paper proposes a robust positioning algorithm that combines the disadvantages of distributed estimation and particle swarm optimization, which can solve the large localization error problem caused by uncertainties in underwater acoustic communication and sampling processes. Considering the presence of ranging anomalies and sampling packet loss in underwater acoustic measurements, a weighted coupling filling method is used to correct the outliers in an underwater acoustic ranging signal. Based on the mapping model from the element array to the underwater acoustic responder, an unconstrained optimization algorithm for one-time localization estimation of underwater acoustic targets was established. Based on the one-time localization estimation results of underwater acoustic targets, an improved multi-particle swarm optimization estimation based on interactive search is proposed, which improves the accuracy of underwater target localization. The numerical results show that the positioning accuracy of the proposed algorithm can be effectively enhanced in cases of distance measurement errors and azimuth measurement errors. Compared with the positioning error before optimization, the positioning error can be reduced after optimization. Additionally, the experiment was carried out in the underwater environment of Hangzhou Qiandao Lake, which verified the positioning performance of the proposed algorithm.

Keywords: underwater acoustics; multi-source sensors; robust positioning; intelligent optimization; experimental testing

Citation: Ge, X.; Zhou, H.; Zhao, J.; Li, X.; Liu, X.; Li, J.; Luo, C. Robust Positioning Estimation for Underwater Acoustics Targets with Use of Multi-Particle Swarm Optimization. *J. Mar. Sci. Eng.* **2024**, *12*, 185. https://doi.org/10.3390/jmse12010185

Academic Editor: Daniel Rouseff

Received: 24 November 2023
Revised: 7 January 2024
Accepted: 12 January 2024
Published: 19 January 2024

1. Introduction

With the continuous improvement of land resource mining technology, people are gradually turning to more abundant marine resources [1]. For marine resource exploration, data are meaningless without knowing the location of underwater targets. Therefore, location-based underwater target services provide special support for many ocean exploration tasks [2], such as underwater remote sensing [3], underwater observation [4], and underwater navigation [5]. Accurately estimating the position of autonomous underwater vehicles (AUVs) has become a major issue in vehicle mission execution [6]. Underwater acoustics usually play an important role in the field of underwater positioning [7]. According to the baseline length, underwater acoustic positioning technology is usually divided into long baseline (LBL) positioning [8], short baseline (SBL) positioning [9], and ultra-short baseline (USBL) positioning [10]. Compared with LBL and SBL positioning systems, a USBL positioning system composed of an underwater acoustic transducer and underwater responder can achieve distributed positioning requirements for underwater targets such as AUVs [11]. However, there are many uncertainties in the underwater environment,

such as signal fluctuations caused by water flow and signal losses caused by faulty equipment [12,13]. Therefore, it is necessary to design an integrated positioning algorithm with higher robustness.

Many scholars have conducted innovative research on underwater acoustics measurements [14]. To address the issue of uncertainties in complex underwater environments, Du et al. established a state model and measurement model based on inertial navigation, and corrected the measurement errors between multiple sensors [15]. With the increase in underwater operation time, measurement models based on inertial navigation have accumulated errors, which leads to unreliable error correcting. In order to reduce the impact of measurement noises on positioning accuracy, a global positioning algorithm for underwater robots based on factor graphs and maximum correlation coefficients was proposed [16]. For the spatial measurement problem, Sklivanitis et al. proposed a rank-based distance complementarity algorithm to solve the spatial measurement problem [17]. With the popularization of machine learning algorithms, a robust data processing method based on online support vector regression was implemented to handle measurement noises, thereby obtaining continuous and consistent localization results [18]. Considering the serious impact of measured uncertainties on underwater positioning accuracy, Saeed et al. formulated the problem of missing pairs of distance and outliers as an optimization problem for semi quadratic minimization, and further proposed a closed form convergent iterative solution that adapts to outliers [19]. Considering the impact of the actual underwater environment on acoustic signals, it is necessary to handle underwater measurement noises.

Many scholars have conducted extensive research on distributed positioning algorithms under various underwater measurement conditions [20]. In order to achieve localization and time synchronization in underwater sensor networks, Gong et al. proposed an AUV assisted linear localization algorithm based on time of arrival (TOA) [21]. However, TOA measurements require strict time synchronization to effectively reduce underwater positioning errors. Chen et al. designed an extended Kalman filtering algorithm based on time difference of arrival (TDOA) for AUV localization, which did not require strict clock synchronization between beacons and AUVs [22]. In order to improve the accuracy of target localization, Yu et al. proposed a least squares localization algorithm based on TOA and angle of arrival (AOA) [23]. Considering the positioning errors of sensor nodes caused by ocean currents, winds, and other factors, Wang et al. proposed a time difference underwater target positioning algorithm based on the weighted total least squares method, which combined prior information from measurement noise variance and self-positioning error variance [24]. Luo et al. proposed underwater data-driven localization estimation using local spatiotemporal nonlinear correlation, which reduced the sensitivity of uncertain noise in the localization solution process [25]. Considering the uncertainty of the actual underwater environment, it is necessary to reduce the impact of ranging and angle measurement errors on the accuracy of underwater positioning.

Since positioning accuracy is the primary issue, intelligent optimization algorithms can be used to further enhance the performance of underwater target localization [26]. Singh et al. proposed a single anchor node target localization method based on H-best particle swarm optimization (HPSO) [27]. In order to provide effective initial values, Wang et al. combined least squares estimation with a genetic algorithm (LSEGA), effectively improving the positioning accuracy [28]. Due to the influence of ocean currents on underwater measurement noises, Hu et al. proposed a localization algorithm that integrates prior knowledge of maximum a posteriori estimation and particle swarm optimization [29]. In addition, intelligent positioning optimization under different measurement types can also effectively improve the accuracy of underwater positioning. Zhou et al. designed a TDOA/AOA data fusion localization method based on a simulated annealing (SA) algorithm to solve the localization problem of underwater targets in large sea areas [30]. Considering that a single SA algorithm cannot obtain the optimal position of underwater targets, Li et al. combined an SA algorithm with a particle swarm optimization algorithm to improve the performance of traditional underwater acoustic localization algorithms [31].

In order to obtain the optimal positioning results of underwater targets, it is necessary to integrate intelligent optimization algorithms.

Underwater target positioning is the foundation of various tasks, including navigation and collaboration. Considering that a single positioning algorithm cannot achieve optimal positioning performance, it is necessary to consider the advantages of integrating different algorithms, including distributed and intelligent optimization. Among them, the main problems are as follows:

(1) Due to the impact of various uncertainties such as ocean noise on acoustic signals, they will inevitably affect the accuracy of underwater target positioning. Therefore, it is necessary to process the errors in underwater acoustic measurements in order to provide a basis for subsequent underwater target calculation.
(2) Considering the issue of distributed positioning algorithms being too sensitive to underwater acoustic measurement noise, especially when there are errors in pitch or azimuth measurements, it is necessary to consider various uncertainties in underwater acoustic measurement and establish a distributed solution model.
(3) Simple positioning algorithms cannot achieve optimal output on a global scale, so it is necessary to introduce artificial intelligence optimization algorithms into distributed positioning solution models to reduce the impact of various uncertain measurements on underwater positioning accuracy.
(4) In view of the above research, these stimulate the current work and provide inspiration for the proposed positioning algorithm underwater, which can solve the unstable positioning performance caused by sparse measurement, especially in the case of outliers. The contributions of this article are as follows.
(5) A padding method with weights coupled depending on the geometric distance and azimuth between the underwater target and the transmission transducer is proposed to deal with measurement noises. Additionally, a threshold detection and measurement correction approach based on time series is suggested to reduce the measurement noise.
(6) Considering the sensitivity of measurement noise to the distributed solution, the underwater target localization problem under uncertainties, including distance and azimuth measurements with a single transmission transducer, is transformed into a constrained total least squares problem.
(7) For improving the positioning performance of underwater targets, an improved multi-particle swarm algorithm with an interaction-based search is used to search for more accurate positions near the initial values. In addition, it is equally important to compare the positioning performance with the existing related algorithms based on simulation and platform experiments.

The remainder of this paper is organized as follows. In Section 2, we give the derivation processes of the proposed robust positioning algorithm in detail. Following that, the numerical evaluations and experimental analyses are carried out in Section 3. Section 4 gives the conclusions.

2. Robust Positioning Estimation for Underwater Acoustics Targets

This paper proposes a positioning method for underwater targets integrating data processing and multi-particle swarm algorithm, as shown in Figure 1. Firstly, a padding method with coupled weights and a measurement correction method were utilized to obtain the processed measurements. Secondly, an unconstrained optimization problem for underwater target positioning was obtained using the regularization term. Thirdly, the optimal estimation of the underwater target was attained through an improved multi-particle swarm algorithm with an interaction-based search.

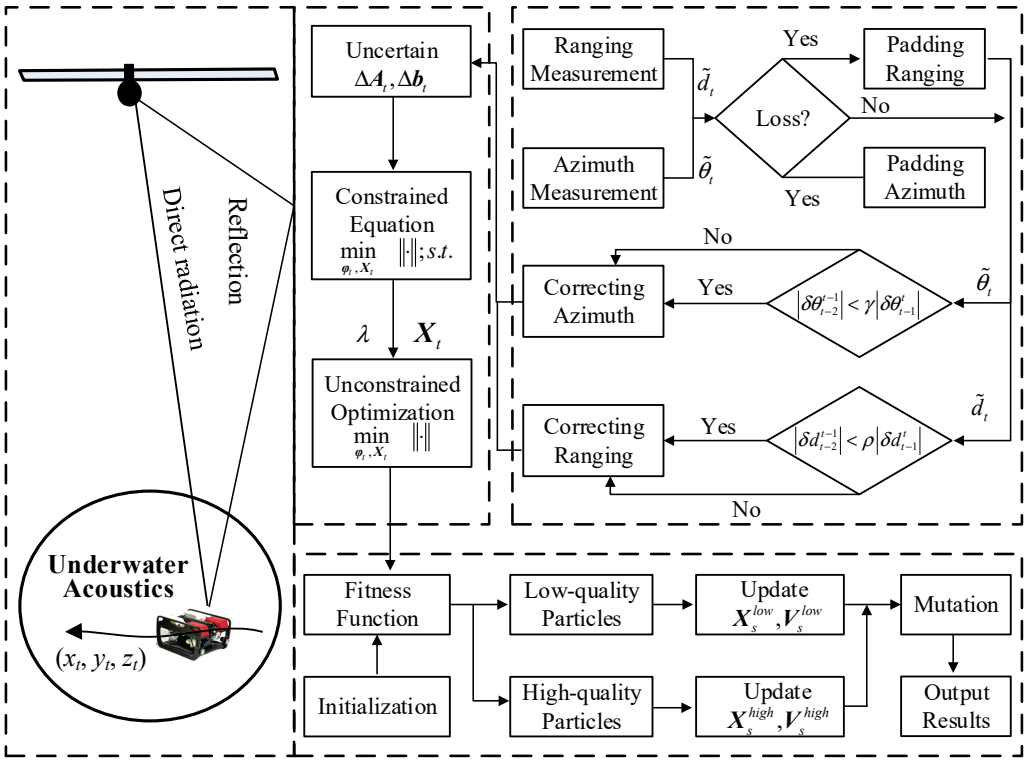

Figure 1. A structure diagram of the proposed positioning algorithm.

Various factors, including the underwater environment, underwater acoustic velocity, sensor installation accuracy, and positioning algorithms, affect the positioning performance of underwater acoustics targets. The following assumptions were made:

Assumption 1. *Due to the time-varying speed and curved propagation path of underwater sound, the small experimental area does not consider the gradient and curvature of* sound speed.

Assumption 2. *Due to environmental limitations, the installation error between the USBL and surface vessel cannot be accurately calibrated. Therefore, the USBL installation error and acoustic beacon will not be considered.*

Assumption 3. *Due to the oblique ranging of USBL acoustic signals through time of arrival, any small asynchrony will affect the accuracy of oblique ranging, and strict time synchronization is assumed.*

2.1. Underwater Signal-Location Mapping Based on Padding and Correcting

At time t, assuming the depth h_t of the underwater target $\boldsymbol{u}_t = [x_t, y_t, h_t]^T$ carrying the transponder is known, where $t = 1, 2, \cdots, T$, there is a single transmission transducer $\boldsymbol{a}$ on the ocean surface at coordinates $[0, 0, 0]^T$. Underwater target $\boldsymbol{u}_t$ can receive signals from a transmission transducer that is located at the origin. The geometric distance d_t between the underwater target $\boldsymbol{u}_t$ and the transmission transducer $\boldsymbol{a}$ can be expressed as

$$d_t = \|\boldsymbol{a} - \boldsymbol{u}_t\| = \sqrt{x_t^2 + y_t^2 + h_t^2} \tag{1}$$

where $\|\cdot\|$ refers to the two-norm. Furthermore, the azimuth θ_t between the underwater target $\boldsymbol{u}_t$ and the transmission transducer $\boldsymbol{a}$ can also be expressed as

$$\theta_t = \tan^{-1}\left(\frac{y_t}{x_t}\right) \tag{2}$$

Squaring both sides of Formula (1) obtains $d_t^2 = x_t^2 + y_t^2 + h_t^2$. Considering Formulas (1) and (2) both contain the squares of the unknown terms x_t and y_t, their corresponding matrices are denoted as

$$\boldsymbol{A}_t \boldsymbol{X}_t = \boldsymbol{b}_t \tag{3}$$

where $\boldsymbol{A}_t = \begin{bmatrix} 1 & 1 \\ \tan^2\theta_t & -1 \end{bmatrix}$, $\boldsymbol{X}_t = \begin{bmatrix} x_t \\ y_t \end{bmatrix}^T$, $\boldsymbol{b}_t = \begin{bmatrix} d_t^2 - h_t^2 \\ 0 \end{bmatrix}$.

Considering the underwater propagation process of a hydroacoustic signal is easily interfered by ocean noises and other signals, the actual ranging value $\widetilde{d}_t$ between the underwater target $\boldsymbol{u}_t$ and the transmission transducer $\boldsymbol{a}$ can be modeled as $\widetilde{d}_t = d_t + \Delta d_t$ at the moment t, where Δd_t is the ranging noise. Moreover, the actual azimuth value $\widetilde{\theta}_t$ between the underwater target $\boldsymbol{u}_t$ and the transmission transducer $\boldsymbol{a}$ can be modeled as $\widetilde{\theta}_t = \theta_t + \Delta\theta_t$ at moment t, where $\Delta\theta_t$ is the angle measurement noise. Since the distance measurement $\widetilde{d}_t$ and azimuth measurement $\widetilde{\theta}_t$ between the underwater target $\boldsymbol{u}_t$ and the transmission transducer $\boldsymbol{a}$ may suffer from outliers or empty measurements, a padding method with weights coupled is established via the distance measurement and the azimuth measurement.

Considering the dynamics of the underwater environment and the robustness of the sensors, there are occasional problems with empty measurement data. This problem will further lead to the non-continuity of underwater target tracking. Thus, the empty measurements are estimated from the known measurements. It is assumed that the distance measurement $\widetilde{d}_t$ is empty and the azimuth measurement $\widetilde{\theta}_t$ is known at time t. A specific relationship between $\widetilde{d}_t$ and $\widetilde{\theta}_t$ can be found according to Formula (3). Therefore, the padded distance measurement $\widetilde{d}_t$ is calculated as $\widetilde{d}_t = \sum_{\substack{i=1 \\ i \neq t}}^{T-1} \widetilde{w}_i^{\theta} \widetilde{d}_i$, where $\widetilde{w}_i^{\theta} = w_i^{\theta} \Big/ \sum_{i=1}^{T-1} w_i^{\theta}$ is denoted as the normalized weight of $w_i^{\theta} = e^{-|\widetilde{\theta}_i - \widetilde{\theta}_t|}$. When the azimuth measurement $\widetilde{\theta}_t$ is empty and the distance measurement $\widetilde{d}_t$ is known, the azimuth measurement $\widetilde{\theta}_t$ is padded as $\widetilde{\theta}_t = \sum_{\substack{i=1 \\ i \neq t}}^{T-1} \widetilde{w}_i^{d} \widetilde{\theta}_i$, where $\widetilde{w}_i^{d} = w_i^{d} \Big/ \sum_{i=1}^{T-1} w_i^{d}$ is denoted as the normalized weight of $w_i^{d} = e^{-|\widetilde{d}_i - \widetilde{d}_t|}$.

Furthermore, considering the underwater targets' motion is sequential, the measurements at time t are similar to the measurements at times $t-1$ and $t-2$. Consequently, the distance measurements $\widetilde{d}_{t-1}$ and $\widetilde{d}_{t-2}$ are used to judge whether the distance measurement $\widetilde{d}_t$ has an outlier at moment t, and the distance measurements $\widetilde{d}_t$ are corrected. The expression for the distance correction value $\hat{d}_t$ is

$$\hat{d}_t = \begin{cases} \widetilde{d}_{t-1} + sign\left(\delta d_{t-1}^t\right) \cdot \left|\delta d_{t-2}^{t-1}\right| & , \left|\delta d_{t-2}^{t-1}\right| < \rho \left|\delta d_{t-1}^t\right| \\ \widetilde{d}_t & , else \end{cases} \tag{4}$$

where $\delta d_{t-2}^{t-1} = \widetilde{d}_{t-2} - \widetilde{d}_{t-1}$; $\delta d_{t-1}^t = \widetilde{d}_{t-1} - \widetilde{d}_t$; ρ denotes the threshold parameter; and $sign(\cdot)$ denotes the sign function. Similarly, the azimuth measurement $\widetilde{\theta}_t$ is judged and corrected, which is expressed as

$$\hat{\theta}_t = \begin{cases} \widetilde{\theta}_{t-1} + sign\left(\delta \theta_{t-1}^t\right) \cdot \left|\delta \theta_{t-2}^{t-1}\right| & , \left|\delta \theta_{t-2}^{t-1}\right| < \gamma \left|\delta \theta_{t-1}^t\right| \\ \widetilde{\theta}_t & , else \end{cases} \tag{5}$$

where $\delta\theta_{t-2}^{t-1} = \widetilde{\theta}_{t-2} - \widetilde{\theta}_{t-1}$; $\delta\theta_{t-1}^t = \widetilde{\theta}_{t-1} - \widetilde{\theta}_t$; and γ denotes the threshold parameter. Obviously, the above correction approach for distance and azimuth measurements can be used only in the case of $t > 2$. Therefore, the measurements of $t = 1$ and $t = 2$ are not corrected here.

2.2. The Optimal Positioning Problem for Underwater Targets

Formula (1) is rewritten according to the distance correction $\hat{d}_t$ in the prior section, which are expressed as

$$x_t^2 + y_t^2 = d_t^2 + 2d_t\Delta\hat{d}_t + \Delta\hat{d}_t^2 - h_t^2 \tag{6}$$

where $\Delta\hat{d}_t = \hat{d}_t - d_t$. Ignoring the squared term $\Delta\hat{d}_t^2$ in the above formula, the above formula can be approximated as

$$x_t^2 + y_t^2 = d_t^2 - h_t^2 + 2d_t\Delta\hat{d}_t \tag{7}$$

By introducing the azimuth correction $\hat{\theta}_t$ into Formula (2), which is rewritten as

$$x_t^2\left(\frac{\tan\theta_t + \tan\Delta\hat{\theta}_t}{1 - \tan\theta_t\tan\Delta\hat{\theta}_t}\right)^2 - y_t^2 = 0 \tag{8}$$

where $\Delta\hat{\theta}_t = \hat{\theta}_t - \theta_t$, when the above formula is extended and the squared term $\tan^2\Delta\hat{\theta}_t$ is ignored, the above formula can be approximated as

$$x_t^2\tan^2\theta_t - y_t^2 + 2x_t^2\tan\theta_t\tan\Delta\hat{\theta}_t + 2y_t^2\tan\theta_t\tan\Delta\hat{\theta}_t = 0 \tag{9}$$

It is clear that the distance correction error $\Delta\hat{d}_t$ and the azimuth correction error $\Delta\hat{\theta}_t$ increase the uncertainty not only in matrix $\boldsymbol{A}_t$, but also in matrix $\boldsymbol{b}_t$. Thus, the matrices $\widetilde{\boldsymbol{A}}_t$ and $\widetilde{\boldsymbol{b}}_t$ with uncertainties can be, respectively, modeled as

$$\begin{cases} \widetilde{\boldsymbol{A}}_t = \boldsymbol{A}_t + \Delta\boldsymbol{A}_t \\ \widetilde{\boldsymbol{b}}_t = \boldsymbol{b}_t + \Delta\boldsymbol{b}_t \end{cases} \tag{10}$$

where $\Delta\boldsymbol{A}_t = \begin{bmatrix} 0 & 0 \\ 2\tan\theta_t\tan\Delta\hat{\theta}_t & 2\tan\theta_t\tan\Delta\hat{\theta}_t \end{bmatrix}$; $\Delta\boldsymbol{b}_t = \begin{bmatrix} 2d_t\Delta\hat{d}_t \\ 0 \end{bmatrix}$.

The noise components of $\Delta\boldsymbol{A}_t$ and $\Delta\boldsymbol{b}_t$ are observed to contain different noise variances based on their individual expressions. As a result, the distance correction error $\Delta\hat{d}_t$ and tangent $\tan\Delta\hat{\theta}_t$ of the azimuth correction error are organized as uncertainty $\boldsymbol{\delta}_t = \left[\Delta\hat{d}_t, \tan\Delta\hat{\theta}_t\right]^T$. With the composition of uncertainty $\boldsymbol{\delta}_t$, matrices $\Delta\boldsymbol{A}_t$ and $\Delta\boldsymbol{b}_t$ can be rewritten as

$$\begin{aligned} \Delta\boldsymbol{A}_t &= \left[\boldsymbol{F}_t^1\boldsymbol{\delta}_t, \boldsymbol{F}_t^2\boldsymbol{\delta}_t\right] \\ \Delta\boldsymbol{b}_t &= \boldsymbol{F}_t^3\boldsymbol{\delta}_t \end{aligned} \tag{11}$$

where $\boldsymbol{F}_t^1 = \begin{bmatrix} 0 & 0 \\ 0 & 2\tan\theta_t \end{bmatrix}$; $\boldsymbol{F}_t^1 = \boldsymbol{F}_t^2$; and $\boldsymbol{F}_t^3 = \begin{bmatrix} 2d_t & 0 \\ 0 & 0 \end{bmatrix}$. Next, the uncertainty $\boldsymbol{\delta}_t$ is converted to $\boldsymbol{\varphi}_t$ using $\boldsymbol{\varphi}_t = \boldsymbol{H}^{-1}\boldsymbol{\delta}_t$, where $\boldsymbol{H}$ is the matrix after the Cholesky decomposition of $E\left(\boldsymbol{\delta}_t\boldsymbol{\delta}_t^T\right)$. Therefore, matrices $\Delta\boldsymbol{A}_t$ and $\Delta\boldsymbol{b}_t$ can be further transformed into

$$\begin{cases} \Delta\boldsymbol{A}_t = \left[\boldsymbol{F}_t^1\boldsymbol{H}\boldsymbol{\varphi}_t, \boldsymbol{F}_t^2\boldsymbol{H}\boldsymbol{\varphi}_t\right] \\ \Delta\boldsymbol{b}_t = \boldsymbol{F}_t^3\boldsymbol{H}\boldsymbol{\varphi}_t \end{cases} \tag{12}$$

The estimation problem of the underwater target's position squared $\boldsymbol{X}_t$ can be solved by constrained total least squares as follows:

$$\begin{aligned} \min_{\boldsymbol{\varphi}_t, \boldsymbol{X}_t} \quad & \|\boldsymbol{\varphi}_t\|^2 \\ s.t. \quad & \begin{bmatrix} \boldsymbol{A}_t & \boldsymbol{b}_t \end{bmatrix}\begin{bmatrix} \boldsymbol{X}_t \\ -1 \end{bmatrix} + \boldsymbol{\Lambda}_t\boldsymbol{\varphi}_t = 0 \end{aligned} \tag{13}$$

where $\boldsymbol{\Lambda}_t = \left(\sum_{q=1}^{2} \boldsymbol{X}_t(q)\boldsymbol{F}_q^t - \boldsymbol{F}_3^t \right) \boldsymbol{H}$. When matrices $\boldsymbol{A}_t$ and $\boldsymbol{b}_t$ are the ill-conditioned matrix, their subtle errors can cause significant fluctuations in the solutions. Thus, the regularized term is introduced, and the above formula can be converted as follows:

$$\begin{aligned} \min_{\boldsymbol{\varphi}_t, \boldsymbol{X}_t} \quad & \|\boldsymbol{\varphi}_t\|^2 + \lambda \|\boldsymbol{X}_t\|^2 \\ s.t. \quad & \begin{bmatrix} \boldsymbol{A}_t & \boldsymbol{b}_t \end{bmatrix} \begin{bmatrix} \boldsymbol{X}_t \\ -1 \end{bmatrix} + \boldsymbol{\Lambda}_t \boldsymbol{\varphi}_t = 0 \end{aligned} \tag{14}$$

where λ refers to the regularized parameter. The above constrained optimization problem is transformed into an unconstrained optimization problem, which is expressed as

$$\min \quad \begin{bmatrix} \boldsymbol{X}_t \\ -1 \end{bmatrix}^T \begin{bmatrix} \boldsymbol{A}_t & \boldsymbol{b}_t \end{bmatrix}^T \left(\boldsymbol{\Lambda}_t^+ \right)^T \boldsymbol{\Lambda}_t^+ \begin{bmatrix} \boldsymbol{X}_t & -1 \end{bmatrix} \begin{bmatrix} \boldsymbol{A}_t \\ \boldsymbol{b}_t \end{bmatrix} + \lambda \boldsymbol{X}_t^T \boldsymbol{X}_t \tag{15}$$

where $\boldsymbol{\Lambda}_t^+$ is the pseudo inverse matrix of $\boldsymbol{\Lambda}_t$.

2.3. Positioning Algorithms Integrated with Intelligent Optimization

The most important feature of the particle swarm optimization (PSO) algorithm is the simpler and fewer adjustment parameters. However, the classical PSO algorithm can fall into the local optimum and has a slow convergence velocity. In order to improve the global search capability, the convergence velocity, and the localization accuracy, this paper proposes an improved multi-particle swarm algorithm, whose improvement steps focus on interactive searching and mutation.

Step 1: Particle swarm initialization. Considering the low search effectiveness after random initialization, the position and velocity of the particles are initialized by combining the least squares preliminary estimation of the underwater target's position squared $\boldsymbol{X}_t$. Then, the initial position $\boldsymbol{X}_s(0)$ and velocity $\boldsymbol{V}_s(0)$ of the particles can be generated by

$$\begin{aligned} \boldsymbol{X}_s(0) &= \hat{\boldsymbol{X}}_t + U(\alpha, \beta) \\ \boldsymbol{V}_s(0) &= \kappa(\boldsymbol{V}_{\max} - \boldsymbol{V}_{\min}) + \boldsymbol{V}_{\min} \end{aligned} \tag{16}$$

where $\hat{\boldsymbol{X}}_t$ denotes the initial value according to the least squares algorithm; $U(\alpha, \beta)$ denotes the random number between α and β; κ is a random number between 0 and 1; and $\boldsymbol{V}_{\max}$ and $\boldsymbol{V}_{\min}$ refer to the maximum and minimum of the particle velocity, respectively.

Step 2: Fitness function. The goodness of the fitness function determines the positioning performance of underwater targets. So as to improve the positioning accuracy of underwater targets, we choose the fitness function as

$$f(\boldsymbol{X}_s(k)) = g_s(k) + \lambda \boldsymbol{X}_s^T(k) \boldsymbol{X}_s(k) \tag{17}$$

where $g_s(k) = \begin{bmatrix} \boldsymbol{X}_s(k) \\ -1 \end{bmatrix}^T \begin{bmatrix} \boldsymbol{A}_t & \boldsymbol{b}_t \end{bmatrix}^T \left(\boldsymbol{\Lambda}_t^+ \right)^T \boldsymbol{\Lambda}_t^+ \begin{bmatrix} \boldsymbol{X}_s(k) & -1 \end{bmatrix} \begin{bmatrix} \boldsymbol{A}_t \\ \boldsymbol{b}_t \end{bmatrix}$. The smaller the fitness function value, the more optimal the particle position.

Step 3: Particle velocity and position update. To ensure the diversity of particle swarm and improve the search efficiency of particle swarm, we divide it into high-quality particles and low-quality particles based on the fitness value. If $f(\boldsymbol{X}_s(k)) \leq f_{mean}$, the particle s is classified as a high-quality particle $\boldsymbol{X}_s^{high}$; otherwise, the particle s is classified as a low-quality particle $\boldsymbol{X}_s^{low}$, where f_{mean} is the average of the total particle swarm's fitness. Simultaneously, different search processes are designed according to the particle subgroups.

Obviously, the fitness of a low-quality particle that deviates from the local optimal solution or the global optimal solution is larger. As a consequence, we expect low-quality particles to tend to global searches, which are used to traverse the entire search region. The

update strategies of a low-quality particle's position $\boldsymbol{X}_s^{low}(k)$ and velocity $\boldsymbol{V}_s^{low}(k)\boldsymbol{V}_s^{low}(k)$ are denoted as

$$\begin{aligned} \boldsymbol{V}_s^{low}(k+1) &= \boldsymbol{V}_s^{low}(k) + 2C_1\left(2 - \frac{2k}{k_{\max}}\right)^2\left(\boldsymbol{Pg} - \boldsymbol{X}_s^{low}(k)\right) \\ \boldsymbol{X}_s^{low}(k+1) &= 2\left(1 - \frac{k}{k_{\max}}\right)\boldsymbol{X}_s^{low}(k) + \boldsymbol{V}_s^{low}(k+1) \end{aligned} \tag{18}$$

where C_1 is a random number between 0 and 1; $\boldsymbol{Pg}$ refers to the global optimum of the particle swarm; and $k_{\max}$ refers to the maximum iteration number.

Since the fitness of a high-quality particle is smaller, which is more locally optimal, it is expected that a high-quality particle can completely search in its local region. Meanwhile, to avoid the high-quality particle focusing on the local search excessively, the global optimum of the particle and the optimum of the low-quality particle subgroup are integrated into the high-quality particle's position and velocity updating strategy, which are expressed as

$$\begin{aligned} \boldsymbol{V}_s^{high}(k+1) &= w\boldsymbol{V}_s^{high}(k) + C_2\left(\boldsymbol{Pb}_s - \boldsymbol{X}_s^{high}(k)\right) + C_3\left(\boldsymbol{Pu} - \boldsymbol{X}_s^{high}(k)\right) \\ \boldsymbol{X}_s^{high}(k+1) &= \boldsymbol{X}_s^{high}(k) + \boldsymbol{V}_s^{high}(k+1) \end{aligned} \tag{19}$$

where C_2 and C_3 are random numbers between 0 and 1.5; $\boldsymbol{Pb}_s$ refers to the individual optimum of the particle s; $\boldsymbol{Pu}$ refers to the optimum of the low-quality particle subgroup; and w is the inertia weight.

Step 4: Mutation. During particle optimization, particles may fall into local optimals caused by the particle swarm optimal solution. For particles falling into local optimums to jump out of local optimums, we need to judge whether the particle $\boldsymbol{X}_s(k)$ is in a local optimum, which is denoted as

$$\begin{cases} H_s^0: & abs((f(\boldsymbol{Pg}) - f(\boldsymbol{X}_s(k)))(f(\boldsymbol{Pg}) - f(\boldsymbol{X}_s(k-1)))) \le \delta \\ H_s^1: & abs((f(\boldsymbol{Pg}) - f(\boldsymbol{X}_s(k)))(f(\boldsymbol{Pg}) - f(\boldsymbol{X}_s(k-1)))) > \delta \end{cases} \tag{20}$$

where δ is the threshold, set as 10^{-4}. If H_s^1 is satisfied, the particle s is not in the local optimum; otherwise, the particle s is in the local optimum. The particle in the local optimum is mutated [32], which is denoted as

$$\boldsymbol{X}_s(k) = \boldsymbol{Pg} + 0.5\left(\boldsymbol{X}_m^{high}(k) - \boldsymbol{X}_n^{high}(k)\right) \tag{21}$$

where $\boldsymbol{X}_m^{high}(k)$ and $\boldsymbol{X}_n^{high}(k)$ are two randomly selected particles from high-quality particles, respectively.

Step 5: Iteration. If the particle fitness $f(\boldsymbol{X}_s(k))$ is less than the individual optimal fitness $f(\boldsymbol{Pb}_s)$, $\boldsymbol{Pb}_s$ is replaced with $\boldsymbol{X}_s(k)$. If the optimal fitness of all individuals is less than the global optimal fitness $f(\boldsymbol{Pg})$, the global optimum $\boldsymbol{Pg}$ is updated. If the iteration number is larger than the maximum iteration number, iteration is stopped and the global optimum $\boldsymbol{Pg}$ is output as the optimal estimation $\widetilde{\boldsymbol{X}}_t$ of $\boldsymbol{X}_t$; otherwise, return to Step 3. Ultimately, according to the azimuth measurement, $\widetilde{\boldsymbol{X}}_t$ is converted to the position estimation $\hat{\boldsymbol{u}}$ of the underwater target, which is expressed as

$$\hat{\boldsymbol{u}} = \left[\sqrt{\boldsymbol{X}(1)}sign(\cos\theta), \sqrt{\boldsymbol{X}(2)}sign(\sin\theta), h\right] \tag{22}$$

In summary, the detailed flow of the proposed algorithm is described in Algorithm 1.

Algorithm 1: Robust positioning estimation for underwater acoustics target

Input: $\widetilde{d}_t$; $\widetilde{\theta}_{t-1}$;
Outputs: $\hat{\boldsymbol{u}}$;
Deploy a transmission transducer $\boldsymbol{a}$
For $t = 1 : T$ **Do**
Pad empty ranges;
Pad empty angles;
If $t > 2$ **Then**
Correct $\widetilde{d}_t$ by Equation (4);
Correct $\widetilde{\theta}_t$ by Equation (5);
Calling Subroutine Optimized positioning algorithm;
End If
End For
Subroutine Optimized positioning algorithm
Primary estimation by LS;
Obtain $\Delta \boldsymbol{A}_t$ and $\Delta \boldsymbol{b}_t$ under uncertainties;
Construct the optimization function by Equation (15);
While $k = 1 : k_{\max}$ until the iteration ends
Particle swarm initialization by Equation (16);
Calculate fitness values;
If $f(\boldsymbol{X}_s(k)) > f_{mean}$ **Then**
Update position $\boldsymbol{X}_s^{low}$ and velocity $\boldsymbol{V}_s^{low}$;
Else
Update position $\boldsymbol{X}_s^{high}$ and velocity $\boldsymbol{V}_s^{high}$;
End If
If H_s^0 is satisfied **Then**
Particle mutation by Equation (21);
End If
$k = k + 1$;
End While
Output estimation $\hat{\boldsymbol{u}}$ by Equation (22).

3. Experimental Results and Performance Evaluation

3.1. Numerical Positioning Performance under Simulation Environment

We carried out the simulation evaluations related to the proposed positioning algorithm with the use of numerical simulations. The underwater area was 300 m × 300 m × 30 m. The transmission transducer $\boldsymbol{a}$ was deployed at the origin. The underwater target moved along a helix trajectory with a 30 m depth during the sampling time. The positioning errors of the underwater target were averaged through 20 Monte-Carlo simulations. The distance measurement errors changed from 0.5% d_t to 2% d_t. The azimuth measurement errors obeyed the Gaussian distributions with mean 0 and changed variance. Other parameter settings are shown in Table 1. The proposed positioning algorithm was compared with three algorithms: LS [23], HPSO [27], and LSEGA [28]. The LS algorithm belongs to the distributed algorithm, while the HPSO and LSEGA algorithms belong to the intelligent optimization algorithm.

Figure 2 shows the positioning error comparison of the algorithm before and after the optimization. With the distance measurement error as 0.5% d_t and the azimuth measurement error variance as 0.1^2, the average positioning errors of the proposed positioning algorithm before and after optimization were 5.29 m and 4.69 m, respectively. These results demonstrate the proposed positioning optimization algorithm can effectively improve the positioning accuracy of underwater targets. As the sampling time increased, the positioning error before and after the optimization became gradually larger. The primary reason is that the underwater target was gradually moving away from the transmission transducer, which led to increasing ranging errors. The distance measurement results directly determine the positioning performance.

Table 1. Parameter settings.

Parameters	Value
Sampling time T	100 s
Distance measurement error	0.5% d_t to 2% d_t
Azimuth error variance	0.1^2 to 0.16^2
Particle number S	100
Maximum iteration $k_{\max}$	100
Maximum velocity $\boldsymbol{V}_{\max}$	5
Minimum velocity $\boldsymbol{V}_{\min}$	-5
Regularization parameter λ	0.05
Distance threshold parameter ρ	0.2
Azimuth threshold parameter γ	0.2

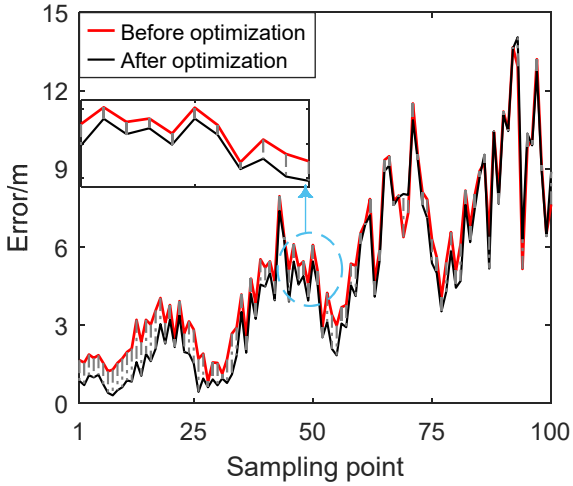

Figure 2. Positioning error comparison of the algorithm before and after the optimization.

Figure 3 shows the positioning results of different positioning algorithms. With the distance measurement error as 0.5% d_t and the azimuth measurement error variance as 0.1^2, the average positioning errors of LS, HPSO, LSEGA, and the proposed positioning algorithm were 5.59, 5.48, 5.28, and 4.69 m, respectively; the minimum positioning errors were 1.06, 1.44, 0.99, and 0.36 m, respectively. These results demonstrate that the proposed algorithm is superior to other algorithms in tracking underwater targets. For the LS, HPSO, and LSEGA algorithms, they had unsatisfactory positioning results during the entire positioning process. The proposed algorithm not only has data processing for distance measurements and azimuth measurements, but also adds an intelligent optimization positioning algorithm, which effectively improves the positioning accuracy and stability for underwater targets.

Figure 4 shows a positioning error comparison of different algorithms under different ratios of distance measurement errors. With the azimuth measurement error variance as 0.1^2, the average positioning errors of the LS, HPSO, LSEGA, and proposed algorithms changed from 5.37, 5.63, 5.38, and 4.72 m to 5.86, 6.41, 6.21, and 5.26 m as the ratio of the distance measurement errors increased from 0.5% to 2%. These results indicate the proposed positioning algorithm has superior positioning results under different distance measurement errors. The HPSO algorithm has random search primaries, resulting in poor positioning performance. For the LS and LSEGA algorithms, the major reason why they had similar positioning results is limited measurement data. However, the proposed algorithm not only handles the measurement data, but also provides positioning process optimization.

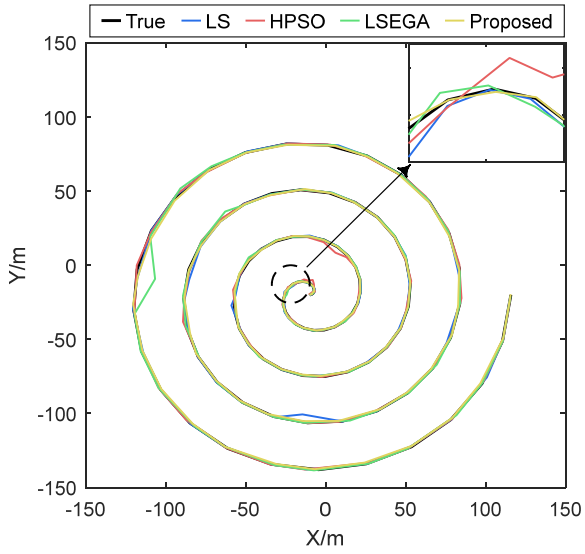

Figure 3. Positioning results of different positioning algorithms.

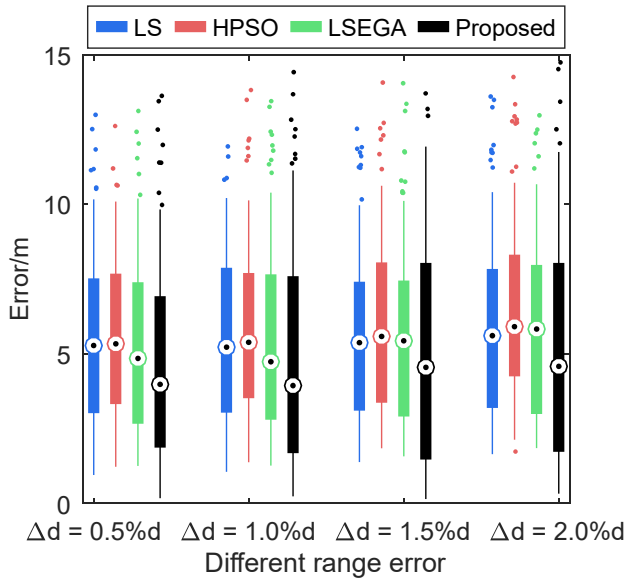

Figure 4. Positioning error comparisons of different algorithms under different ratios of distance measurement errors.

Figure 5 shows the positioning performance comparison of different positioning algorithms under different azimuth measurement error variances. With the ratio of distance measurement errors as 0.5%, the average positioning errors of the LS, HPSO, LSEGA, and proposed algorithms changed from 5.39, 5.64, 5.37, and 4.97 m to 8.22, 8.89, 8.64, and 7.64 m as the azimuth measurement error variance increased from 0.1^2 to 0.16^2. Obviously, the proposed positioning algorithm still had superior positioning performance than the others under the increasing variance in azimuth measurement errors. Moreover, the azimuth measurement accuracy also strongly determines the positioning performance of different algorithms. Regarding the LS, HPSO, and LSEGA algorithms, the proposed positioning algorithm is affected by the azimuth measurement errors at a lower level, which is mainly due to the optimization of the azimuth measurement results added in the proposed positioning algorithm.

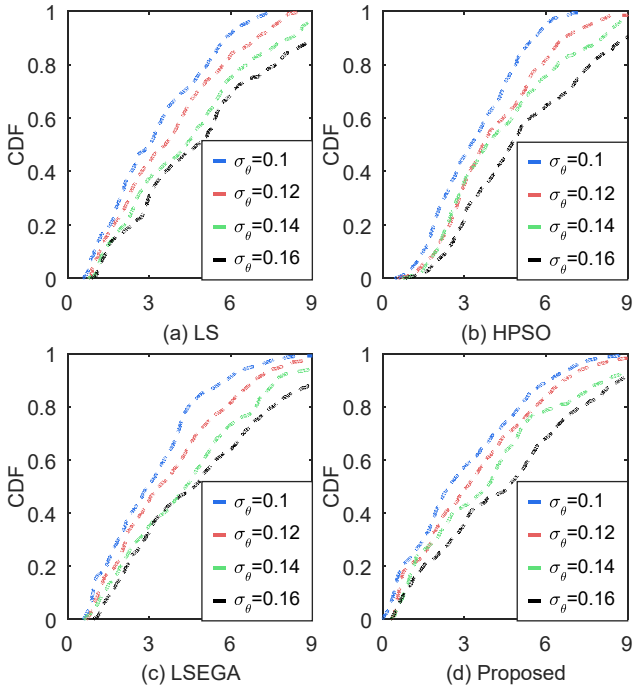

Figure 5. Positioning performance comparison of different positioning algorithms under different azimuth measurement error variances.

Figure 6 shows the computation time of different positioning algorithms. The computation time is the average of 50 Monte Carlos. With the distance measurement error as 0.5% d_t and the azimuth measurement error variance as 0.1^2, the average computation times of LS, HPSO, LSEGA, and the proposed positioning algorithm were 0.05, 0.13, 0.25, and 0.41 s, respectively. Since the LS algorithm belongs to the distributed algorithm, the computation time was the lowest. The HPSO and LSEGA algorithms utilize the intelligent optimization algorithm, resulting in longer computation times. The proposed algorithm had the highest computational time, which is primarily attributable to the additional data processing stage and intelligent positioning optimization. Compared to other algorithms, the proposed positioning algorithm had the best positioning accuracy despite the increase in computation time. As processors continue to advance, longer computation times can be effectively reduced.

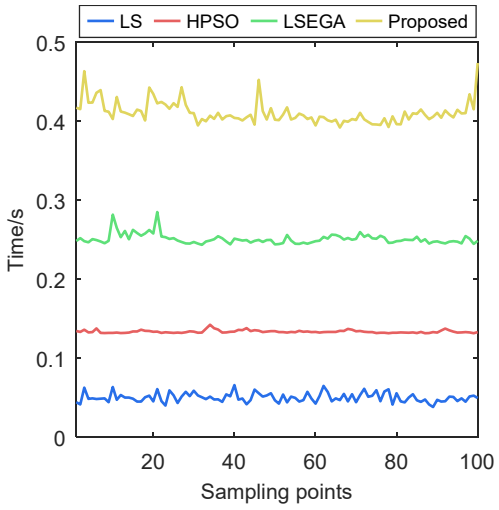

Figure 6. Computation time of different positioning algorithms.

3.2. Experimental Positioning Performance in Underwater Environments

For testing the positioning performance of the proposed algorithm, we carried out the experimental test in Hangzhou Qiandao Lake, as shown in Figure 7. The ultra-short baseline used was a Sonardyne Type 8024 high-frequency ultra-short baseline, with a frequency of 35–55 KHz, matched with Sonardyne Type 7986 acoustic beacon, with an operating range of 500 m and a measurement accuracy of 0.5% slant distance. The transponder received the acoustic signal from the transmission transducer and acquired the distance and azimuth. The measured data were transmitted to the base station located on the ship for positioning calculations.

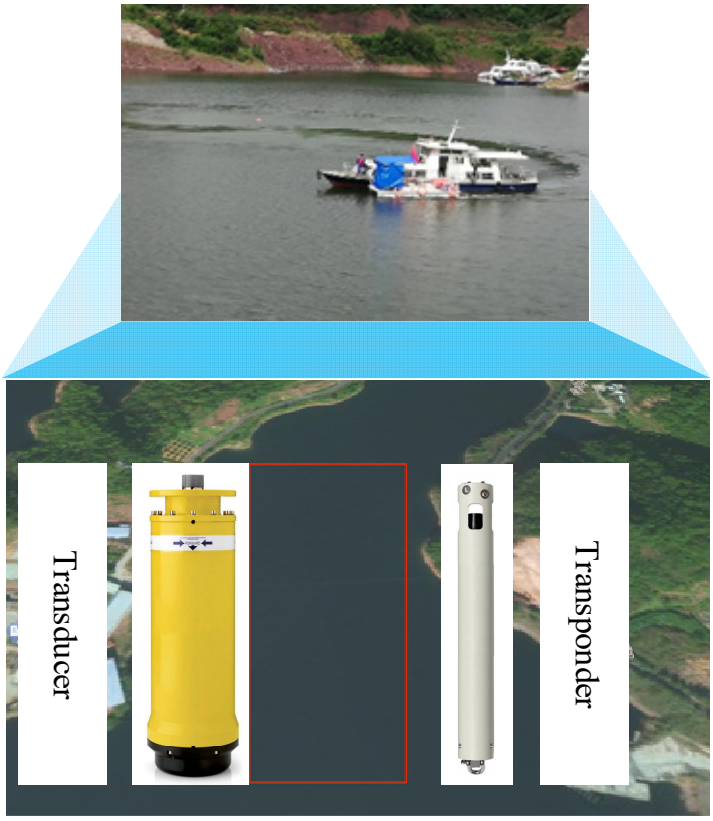

Figure 7. Actual positioning environment.

Figure 8 shows the positioning experiment data and positioning results of the underwater target. Figure 8a shows the variation in distance measurements between the transmission transducer and the transponder during the entire sampling time. As the sampling time increased, the distance measurements gradually increased, which indirectly suggested the underwater measured point with the transponder was gradually moving away from the ship with the transmission transducer. Figure 8b shows the variation in the azimuth measurements between the transmission transducer and the transponder during the entire sampling time. During the entire sampling time, the azimuth measurements were alternatively transformed in positive and negative directions. Figure 8c shows the depth variation of the underwater measured point during the entire sampling time, and the whole variation was similar to the variation in distance measurements. Figure 8d shows the location estimation of the underwater measured point using the proposed algorithm in this experiment. The position estimation of the underwater measured point was continuously changing without unexpected variations during the entire sampling time, indicating the proposed algorithm has better localization robustness.

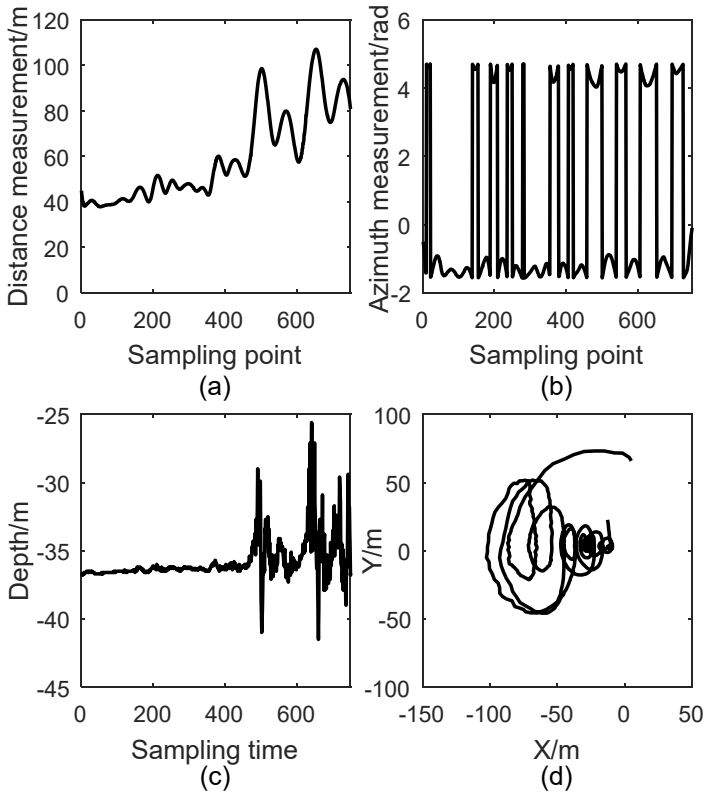

Figure 8. Positioning experiment data and positioning results of the underwater target. (**a**) The distance between transducer and transponder; (**b**) The azimuth between transducer and transponder; (**c**) The changed depth of measured point; (**d**) The estimated locations of measured point.

4. Conclusions

This paper proposes a robust positioning estimation for underwater acoustics targets with the use of multi-particle swarm optimization, which is utilized for underwater target localization under numerous uncertainties. The proposed positioning algorithm uses the relationship between measurements to pad and correct the measurements, and then solves the unconstrained optimization problem using improved multi-particle swarm optimization to position the underwater target. Compared with the LS, HPO, and LSEGA algorithms, the simulation results indicate the proposed algorithm has better positioning accuracy and robustness. The positioning error of the proposed algorithm after optimization was reduced by 0.60 m, which demonstrates the feasibility and superiority of the improved multi-particle swarm algorithm. As the azimuth measurement error variance increased to 0.16^2, the average positioning errors of LS, HPSO, LSEGA, and the proposed algorithm increased by 2.83 m, 3.25 m, 3.27 m, and 2.67 m. Similarly, the increased distance measurement errors also increased the positioning algorithm errors. Furthermore, we performed positioning experiments for the underwater measured point in Hangzhou Qiandao Lake, aiming to test the proposed algorithm's reliability. These results illustrate the proposed positioning algorithm has superior positioning performance with a single transmission transducer, although it adds some computational time.

Due to the fact that underwater sound velocity measurement is the foundation of underwater target localization, subsequent research will introduce intelligent algorithms to correct sparse effective sound velocity and integrate sensors, including inertial measurement units and Doppler velocimeters, to construct a combined navigation and positioning system. High order filtering algorithms will be used to enhance the performance of underwater target positioning.

Author Contributions: Conceptualization, X.G.; methodology, H.Z.; software, C.L.; validation, X.L. (Xiaowei Li); formal analysis, X.L. (Xinyu Liu); investigation, J.L.; resources, X.G.; data curation, J.Z.; writing—original draft preparation, X.G.; writing—review and editing, C.L.; visualization, J.Z.; supervision, H.Z.; project administration, X.G. All authors have read and agreed to the published version of the manuscript.

Funding: This research received no external funding.

Institutional Review Board Statement: Not applicable.

Informed Consent Statement: Not applicable.

Data Availability Statement: Data are contained within the article.

Acknowledgments: The authors would like to thank the anonymous reviewers for their helpful comments which improved the quality of the paper.

Conflicts of Interest: The authors declare no conflicts of interest.

References

1. Qiao, G.; Muhammad, A.; Muzzammil, M.; Khan, M.S.; Tariq, M.O.; Khan, M.S. Addressing the directionality challenge through RSSI-Based multilateration technique, to localize nodes in underwater WSNs by using magneto-inductive communication. *J. Mar. Sci. Eng.* **2022**, *10*, 530. [CrossRef]
2. Luo, C.M.; Cao, Y.X.; Xin, G.G.; Wang, B.; Lu, E.; Wang, H.L. Three-dimensional coverage optimization of underwater nodes under multiconstraints combined with water flow. *IEEE Internet Things J.* **2022**, *9*, 2375–2389. [CrossRef]
3. Pourkabirian, A.; Kooshki, F.; Anisi, M.H.; Jindal, A. An accurate RSS/AoA-based localization method for internet of underwater things. *Ad Hoc Netw.* **2023**, *145*, 103177. [CrossRef]
4. Liu, L.; Zhang, L.C.; Pan, G.; Zhang, S. Robust yaw control of autonomous underwater vehicle based on fractional-order PID controller. *Ocean Eng.* **2022**, *257*, 111493. [CrossRef]
5. Liu, Y.; Wang, Y.M.; Chen, C.; Liu, C.X. Underwater wireless sensor network-based localization method under mixed Line-of-Sight/Non-Line-of-Sight conditions. *J. Mar. Sci. Eng.* **2023**, *11*, 1642. [CrossRef]
6. Zhang, L.C.; Wang, T.H.; Zhang, F.H.; Xu, D.M. Cooperative localization for multi-AUVs based on GM-PHD filters and information entropy theory. *Sensors* **2017**, *17*, 2286. [CrossRef] [PubMed]
7. Fabijanic, M.; Kapetanovic, N.; Miskovic, N. Autonomous visual fish pen inspections for estimating the state of biofouling buildup using ROV. *J. Mar. Sci. Eng.* **2023**, *529*, 1873. [CrossRef]
8. Song, J.; Li, W.Q.; Zhu, X.W.; Dai, Z.Q.; Ran, C.X. Underwater adaptive height-constraint algorithm based on SINS/LBL tightly coupled. *IEEE Trans. Instrum. Meas.* **2022**, *71*, 1–9. [CrossRef]
9. Almeida, J.; Matias, B.; Ferreira, A.; Almeida, C.; Martins, A.; Silva, E. Underwater Localization System Combining iUSBL with Dynamic SBL in VAMOS! Trials. *Sensors* **2020**, *20*, 4710. [CrossRef]
10. Guo, H.R.; Qian, Z.W.; Wang, X.J.; Sun, W.Z.; Jie, L.; Zhai, J.S. A robust attitude estimation algorithm for seabed inverted ultra-short baseline. *Ocean Eng.* **2023**, *280*, 114534. [CrossRef]
11. Li, Y.H.; Ruan, R.Z.; Zhou, Z.P.; Sun, A.Q.; Luo, X.A. Positioning of unmanned underwater vehicle based on autonomous tracking buoy. *Sensors* **2023**, *23*, 4398. [CrossRef] [PubMed]
12. Yi, J.; Tang, J.; Yuan, F.; Qiao, G.; Dai, D. Non-Uniform clustering algorithm for UWSNs based on energy equalization. *Sensors* **2023**, *23*, 5466. [CrossRef] [PubMed]
13. Luo, C.M.; Wang, B.; Cao, Y.X.; Xin, G.F.; He, C.; Ma, L. A hybrid coverage control for enhancing UWSN localizability using IBSO-VFA. *Ad Hoc Netw.* **2021**, *123*, 102694. [CrossRef]
14. Gehrmann, R.A.S.; Barclay, D.R.; Johnson, H.; Shajahan, N.; Nolet, V.; Davies, K.T.A. Ambient noise levels with depth from an underwater glider survey across shipping lanes in the Gulf of St. Lawrence, Canada. *J. Acoust. Soc. Am.* **2023**, *154*, 1735–1745. [CrossRef]
15. Du, Z.Q.; Chai, H.Z.; Xiang, M.Z.; Zhang, F.; Wang, Z.Y. Resilient model of multi-UUVs cooperative localization for detection of sensor fault and outliers. *Ocean Eng.* **2022**, *266*, 113216. [CrossRef]
16. Fan, S.W.; Zhang, Y.; Hao, Q.; Jiang, P.; Yu, C.Y.; Yu, F. Cooperative positioning for multi-AUVs based on factor graph and maximum correntropy. *IEEE Access* **2019**, *7*, 153327–153337. [CrossRef]
17. Sklivanitis, G.; Markopoulos, P.P.; Pados, D.A.; Diamant, R. Robust graph localization for underwater acoustic networks. In Proceedings of the 2021 Fifth Underwater Communications and Networking Conference (UComms), Lerici, Italy, 31 August–2 September 2021; pp. 1–5.
18. Liu, X.J.; Liu, X.X.; Zhang, T.W.; Wang, Q.M. Robust data cleaning methodology using online support vector regression for ultra-short baseline positioning system. *Rev. Sci. Instrum.* **2019**, *90*, 124901. [CrossRef]
19. Saeed, N.; Al-Naffouri, T.Y.; Alouini, M.-S. Outlier detection and optimal anchor placement for 3D underwater optical wireless sensor networks localization. *IEEE Trans. Commun.* **2019**, *67*, 611–622. [CrossRef]

20. Sathish, K.; Chinthaginjala, R.; Kim, W.; Rajesh, A.; Corchado, J.M.; Abbas, M. Underwater wireless sensor networks with RSSI-Based advanced efficiency-driven localization and unprecedented accuracy. *Sensors* **2023**, *23*, 6973. [CrossRef]
21. Gong, Z.J.; Li, C.; Jiang, F. AUV-Aided joint localization and time synchronization for underwater acoustic sensor networks. *IEEE Signal Process Lett.* **2018**, *25*, 477–481. [CrossRef]
22. Chen, H.F.; Zhang, L.Y.X.; Liu, F.; Lv, C.L.; Xie, L.; Xiong, S.J.; Wang, H.J.; Yang, S.Q.; Xu, W. Sea experiment of positioning underwater mobile vehicles using multiple surface beacons. In Proceedings of the Global Oceans 2020: Singapore—U.S. Gulf Coast, Biloxi, MS, USA, 5–30 October 2020; pp. 1–6.
23. Yu, K.G. 3-D localization error analysis in wireless networks. *IEEE Trans. Wirel. Commun.* **2007**, *6*, 3472–3481.
24. Wang, L.; Shen, X.H.; Liu, X.; Hua, F.; Wang, H.Y. Target localization based on weighted total least squares in underwater acoustic networks. In Proceedings of the 2019 IEEE International Conference on Signal Processing, Communications and Computing (ICSPCC), Dalian, China, 20–22 September 2019; pp. 1–5.
25. Luo, C.M.; Wang, L.X.; Yang, X.D.; Xin, G.F.; Wang, B. Underwater data-driven positioning estimation using local spatiotemporal nonlinear correlation. *IEEE/CAA J. Autom. Sin.* **2023**, *10*, 1775–1777. [CrossRef]
26. Kaliraj, S.; Hariharan, B.; Sivakumar, V.; Josephin, J.S.F.; Siva, R.; Prakash, P.N.S. Doppler shift with archimedes optimization algorithm for localizing unknown nodes in underwater sensor networks. *Int. J. Commun. Syst.* **2023**, *36*, e5604.
27. Singh, P.; Khosla, A.; Kumar, A.; Khosla, M. Optimized localization of target nodes using single mobile anchor node in wireless sensor network. *AEU-Int. J. Electron. Commun.* **2018**, *91*, 55–65. [CrossRef]
28. Wang, S.J.; Wang, S.B.; Liu, W.L.; Tian, Y. A study on the optimization nodes arrangement in UWB localization. *Measurement* **2020**, *163*, 108056. [CrossRef]
29. Hu, K.Y.; Song, X.L.; Sun, Z.W.; Luo, H.J.; Guo, Z.W. Localization based on MAP and PSO for drifting-restricted underwater acoustic sensor networks. *Sensors* **2018**, *19*, 71. [CrossRef]
30. Zhou, Y.F.; Wang, Y.M.; Nie, R.X.; Cheng, Q.; Zhu, G.L. Optimal Location Method of Spontaneous Data Fusion based on TDOA /AOA. In Proceedings of the 2021 OES China Ocean Acoustics (COA), Harbin, China, 14–17 July 2021; pp. 885–889.
31. Li, J.Q.; Li, L.; Yu, F.J.; Ju, Y.; Ren, J.W. Application of simulated annealing particle swarm optimization in underwater acoustic positioning optimization. In Proceedings of the OCEANS 2019—Marseille, Marseille, France, 17–20 June 2019; pp. 1–4.
32. Li, W.; Meng, X.; Huang, Y.; Fu, Z.H. Multipopulation cooperative particle swarm optimization with a mixed mutation strategy. *Inf. Sci.* **2020**, *529*, 179–196. [CrossRef]